Characterization of the TolB–Pal trans-envelope complex from *Xylella fastidiosa* reveals a dynamic and coordinated protein expression profile during the biofilm development process

Clelton A. Santos [a], Richard Janissen [b,1], Marcelo A.S. Toledo [a], Lilian L. Beloti [a], Adriano R. Azzoni [c], Monica A. Cotta [b], Anete P. Souza [a,d,*]

[a] *Centro de Biologia Molecular e Engenharia Genética, Universidade Estadual de Campinas, Campinas, SP, Brazil*
[b] *Instituto de Fisica Gleb Wataghin, Universidade Estadual de Campinas, Campinas, SP, Brazil*
[c] *Departamento de Engenharia Química, Escola Politécnica, Universidade de São Paulo, São Paulo, SP, Brazil*
[d] *Departamento de Biologia Vegetal, Instituto de Biologia, Universidade Estadual de Campinas, Campinas, SP, Brazil*

ARTICLE INFO

ABSTRACT

The intriguing roles of the bacterial Tol–Pal trans-envelope protein complex range from maintenance of cell envelope integrity to potential participation in the process of cell division. In this study, we report the characterization of the XfTolB and XfPal proteins of the Tol–Pal complex of *Xylella fastidiosa*. *X. fastidiosa* is a major plant pathogen that forms biofilms inside xylem vessels, triggering the development of diseases in important cultivable plants around the word. Based on functional complementation experiments in *Escherichia coli tolB* and *pal* mutant strains, we confirmed the role of *xftolB* and *xfpal* in outer membrane integrity. In addition, we observed a dynamic and coordinated protein expression profile during the *X. fastidiosa* biofilm development process. Using small-angle X-ray scattering (SAXS), the low-resolution structure of the isolated XfTolB–XfPal complex in solution was solved for the first time. Finally, the localization of the XfTolB and XfPal polar ends was visualized via immunofluorescence labeling in vivo during bacterial cell growth. Our results highlight the major role of the components of the cell envelope, particularly the TolB–Pal complex, during the different phases of bacterial biofilm development.

© 2015 Elsevier B.V. All rights reserved.

1. Introduction

One of the most important stages of niche colonization by biofilm-forming bacteria is adherence to the superficies to be colonized [1,2]. The adhesion stage requires the expression of a range of proteins, including adhesin, as well as the increased expression of lipopolysaccharide on the cell surface [3,4]. Thus, the cell envelope and all the proteins responsible for its maintenance are key elements of the success of niche- and/or host-specific colonization by these microorganisms.

The Tol–Pal system is ubiquitous in Gram-negative bacteria and is associated with cell envelope integrity [5,6]. The genes encoding the proteins of this system are typically organized into operons and include *tolQ, tolR* and *tolA*, which encode proteins located in the inner membrane; *ybgC* and *ybgF*, which encode products of unknown function;

and the *pal* and *tolB* genes [7–9]. Pal is a peptidoglycan-associated outer membrane-anchored lipoprotein that resides in the periplasmic space and is strongly associated with the peptidoglycan layer through a conserved α-helical motif [10,11]. TolB (translocation protein TolB) is an allosteric β-propeller protein that acts in the bacterial periplasmic space and may interact with other proteins, including Pal [12–15] and the cell-killing proteins categorized as group A colicins [16–18].

Null mutants of the *tol–pal* genes exhibit a 'leaky-membrane' phenotype with a tendency to form vesicles on the outer membrane, reduced expression of lipopolysaccharide on the cell surface, defects in cell division and increased sensitivity to antibiotics and detergents [5,19,20]. Gerding et al. [21] proposed that the Tol–Pal complex is part of the cell division machinery of Gram-negative bacteria and is required for proper invagination of the cell envelope during cell constriction in *Escherichia coli*. However, while the Tol–Pal complex clearly plays an important role in the maintenance and integrity of the bacterial cell envelope, the physiological role of this protein complex has not been fully elucidated.

The *tol–pal* genes have been associated with the pathogenesis of several bacteria, including *Salmonella typhimurium*, *Vibrio cholerae*, *Erwinia chrysanthemi*, and *Burkholderia cenocepacia* [22–26]. In the biofilm-forming bacterium *Pseudomonas aeruginosa*, *tolB* is essential

for bacterial growth, resistance and pathogenicity [27], and *tolA* is up-regulated during biofilm development [28]. Consistent with its apparent function, *tolB* is required for the growth of *E. coli* at high hydro-static pressure (40 mPa) [29]. More recently, *pal* expression was observed during the infective stage of *Lawsonia intracellularis*, a fastidious, microaerophilic obligate intracellular bacterium [30]. These results illustrate the critical role of this protein system in bacterial virulence.

Here, we report the characterization of the XfTolB and XfPal proteins of the Tol–Pal cell envelope complex of the plant pathogen *Xylella fastidiosa*. Our findings confirm the involvement of the XfTolB and XfPal proteins in membrane integrity and demonstrate dynamic, coordinated XfTolB and XfPal expression during the *X. fastidiosa* biofilm development process. Using small-angle X-ray scattering (SAXS), the low-resolution structure of the XfTolB–XfPal complex in solution was solved for the first time. In addition, XfTolB and XfPal were visualized during *X. fastidiosa* growth in vivo via immunolabeling. Our results highlight the major role of the components of the cell envelope, partic-ularly the TolB–Pal complex, during the growth of the biofilm-forming plant pathogen *X. fastidiosa*.

2. Material and methods

2.1. Bacterial strains, plasmids and culture conditions

The bacterial strains and plasmids used in the present study are described in Table 1. The *X. fastidiosa* 9a5c strain [31] and *E. coli* strains DH5α (Invitrogen, Carlsbad, CA, USA), BL21 (DE3) (Novagen, Madison, WI, USA), BW25113 [32], JW5100 and JW0731 [33] have been described previously. *X. fastidiosa* was cultured in periwinkle wilt (PW) medium [34] at 130 rpm and 28 °C, and the *E. coli* strains were grown in LB or BHI broth at 200–300 rpm and 25–37 °C. When appropriate, the medium was supplemented with 30 μg·mL^{-1} kanamycin and/or 100 μg·mL^{-1} ampicillin. The medium was also occasionally supple-mented with L-arabinose, isopropyl-β-D-thiogalactopyranoside (IPTG) and/or sodium dodecyl sulfate (SDS) as indicated. XfTolB and XfPal expression constructs were prepared using standard molecular biology techniques [35] and the plasmids pET29a (Novagen, Madison, WI, USA) and pBAD24 [36]. Gene expression from the T7 promoter in pET29a was induced by the addition of 0.4 mM IPTG, while gene expression from the *araC*P$_{BAD}$ promoter in pBAD24 was induced by 0.2% (w/v) L-arabinose.

2.2. Cloning, expression and purification of XfTolB and XfPal

The coding sequence of the XfTolB protein (ORF Xf1625; GenBank accession number: WP_023906495.1) lacking the signal peptide sequence (amino acid residues 1 to 23) was amplified by PCR from genomic DNA of the *X. fastidiosa* 9a5c strain using the specific oligonu-cleotides Xf1625F (5′-CCAAACATATGACGAAA TTTCCACGCTGG-3′) and Xf1625R (5′-AAACTCGAGATGTACGCTCCGG TAAGGCCC-3′), which contain restriction sites for the enzymes *Nde*I and *Xho*I, respectively. The PCR amplification product was cloned into the expression vector pET29a to enable expression as a fusion with a C-terminal tag contain-ing six histidine residues (His$_6$-tag). The absence of base substitutions in the recombinant plasmid was evaluated by DNA sequencing. XfTolB was overexpressed in *E. coli* BL21 (DE3). The cells were cultured at 37 °C with shaking at 300 rpm in 1 L of LB broth containing kanamycin (30 μg mL^{-1}) until an OD$_{600}$ of 0.6–0.8 was reached. Expression of the recombinant protein was induced by adding 0.4 mM IPTG, followed by cultivation for 16 h at 25 °C and 200 rpm. The culture was then centri-fuged (3000 *g*, 15 min, 4 °C), and the cells were resuspended in 50 mL of buffer A (50 mM Tris–Cl pH 6.5 and 300 mM NaCl) containing 1 mg·mL^{-1} lysozyme and 2 mM phenylmethanesulfonyl fluoride (PMSF; Sigma-Aldrich, St. Louis, MO, USA). The cells were disrupted by sonication, and the soluble fraction was collected by centrifugation (20,000 *g*, 40 min, 4 °C). XfTolB was purified by nickel affinity chroma-tography using Ni-NTA resin (Qiagen, Germany) equilibrated with buffer A. The purified protein was eluted using an imidazole gradient (0 to 500 mM). The purity of the XfTolB protein samples was estimated by SDS-PAGE.

The cloning, expression and purification of XfPal lacking its signal peptide were performed using the protein refolding protocol previously described by Santos et al. [37]. The concentrations of the recombinant purified His$_6$-tag XfTolB and XfPal proteins were determined spectro-photometrically using calculated molar extinction coefficients (ε$_{280}$) of 55,810 and 16,180 M^{-1} cm^{-1}, respectively.

2.3. Functional complementation of xftolB and xfpal in knockout E. coli strains

The involvement of XfTolB and XfPal in membrane integrity was assessed in vivo using a functional complementation assay based on the SDS sensitivity of *tolB*$^-$ and *pal*$^-$ *E. coli* mutants [33]. The full-length *xftolB* and *xfpal* genes were cloned into the pBAD24 vector

Table 1
Bacterial strains and plasmids used.

Strain or plasmid	Relevant genotype and/or characteristics	Reference or source
Xylella fastidiosa		
X. fastidiosa 9a5c	Gram-negative, biofilm-forming isolate that causes citrus variegated chlorosis (CVC) in orange	[31]
Escherichia coli		
DH5α	F$^-$ *endA*1 *glnV*44 *thi*-1 *recA*1 *relA*1 *gyrA*96 *deoR* *nupG* Φ80*dlacZ*ΔM15 Δ(*lacZYA*-*arg*F)U169, *hsdR*17, λ$^-$	Invitrogen
BL21(DE3)	F$^-$ *ompT* *gal* *dcm* *lon* *hsd*S$_B$ λ(DE3)	Novagen
BW25113	F$^-$ Δ*lacZ*4787(::*rrnB*3) *hsdR*514 Δ(*araBAD*)567 Δ(*rhaBAD*)568 *rph*-1 λ$^-$	[32]
BW25113-pBAD24	BW25113 with the arabinose-inducible empty vector pBAD24	This study
JW5100	BW25113 Δ*tolB*789::*kan*	[33]
JW5100-pBAD24	JW5100 with the arabinose-inducible empty vector pBAD24	This study
JW5100-pBAD24-*xftolB*	JW5100 with an arabinose-inducible copy of *xftolB* in pBAD24	This study
JW0731	BW25113 Δ*pal*790::*kan*	[33]
JW0731-pBAD24	JW0731 with the arabinose-inducible empty vector pBAD24	This study
JW0731-pBAD24-*xfpal*	JW0731 with an arabinose-inducible copy of *xfpal* in pBAD24	This study
Plasmid		
pET29a	Commercial vector carrying the T7 promoter system IPTG-inducible, kan^R	Novagen
pBAD24	Vector carrying the *araC*P$_{BAD}$ arabinose-inducible promoter system and a Shine–Dalgarno box for the translation start codon; Amp^R	[36]
pBAD24-*xftolB*	pBAD24 carrying the *xftolB* coding sequence cloned between the *Nco*I and *Sal*I restriction sites	This study
pBAD24-*xfPal*	pBAD24 carrying the *xfpal* coding sequence cloned between the *Nco*I and *Sal*I restriction sites	This study

using the oligonucleotides XfTolB$_{BAD}$F (5′-TA<u>CCATGG</u>GTACGAAATTTC CACGCTG-3′), XfTolB$_{BAD}$R (5′-ACT<u>GTCGAC</u>TTAATGTACGCTCCGGTA-3′), XfPal$_{BAD}$F (5′-TACCATGGCACCAACTGTTTCTAC-3′), and XfPal$_{BAD}$R (5′-CGTGTCGACTTACTTCGCTGTATAG-3′). The forward and reverse primers contained *Nco*I and *Sal*I restriction sites, respectively. The empty pBAD24 vector or the pBAD24-*xftolB* or pBAD24-*xfpal* construct was transformed into *E. coli* JW5100 (*tolB* deletion mutant) or JW0731 (*pal* deletion mutant), which were derived from the wild-type BW25113 strain (Table 1). The wild-type and deletion mutant strains were provided by the National BioResource Project (NIG Japan). The SDS growth inhibitory effect was assessed using an adapted Kirby–Bauer disc diffusion test. Briefly, the strains (wild-type, *tolB*⁻ and *pal*⁻ containing empty vector or the *xftolB* or *xfpal* construct) were grown overnight in LB containing 100 μg·mL⁻¹ ampicillin or 30 μg·mL⁻¹ kanamycin (depending on the strain) at 37 °C and 300 rpm. The cultures were then diluted 100-fold in Brain–Heart Infusion (BHI; HiMedia, Mumbai, India) medium supplemented with the appropriate antibiotic and grown at 37 °C and 300 rpm to an OD$_{600}$ of 0.8. After growth, 200 μL of cells of each culture was individually inoculated on BHI plates supplemented with 0.2% (w/v) L-arabinose. A 5-mm-diameter filter paper disc with 5 μL of 10% (w/v) SDS was placed on the plates, and the SDS-associated phenotype was analyzed following incubation of the plates at 37 °C overnight. The effect of 0.2% (w/v) SDS on cell growth was evaluated by measuring the turbidity (OD$_{600}$) every 15 min for 8 h of bacterial growth (wild-type, mutants and mutants complemented with *xftolB* or *xfpal* construct) in BHI liquid culture. All experiments were performed in triplicate.

2.4. Western blotting analyses of XfTolB and XfPal expression during X. fastidiosa biofilm formation

The *X. fastidiosa* 9a5c strain was used to obtain different developmental phases of *X. fastidiosa* biofilm, and planktonic cells of the same age corresponding to each biofilm phase were obtained using a protocol established by de Souza et al. [38]. Polyclonal anti-XfTolB and anti-XfPal antibodies were produced by Rheabiotech (Campinas, SP, Brazil) and were used in XfTolB and XfPal immunoblotting during planktonic growth or *X. fastidiosa* biofilm formation. For western blot analyses, total protein was extracted from *X. fastidiosa* at different stages of biofilm formation and planktonic cells and analyzed and normalized as described by Santos et al. [39]. Approximately 5 μg of total *X. fastidiosa* protein from each sample was used for the immunodetection experiments. The polyclonal anti-Hsp70/Hsc70 Global (StressMarq Biosciences, Victoria, BC, Canada) antibody for the detection of the bacterial DnaK protein (68 kDa) was used as a loading control.

2.5. Immunofluorescence labeling of XfTolB and XfPal

The immunofluorescence-based localization of the XfTolB and XfPal proteins in the *X. fastidiosa* 9a5c cell envelope was performed using the polyclonal anti-XfTolB and anti-XfPal antibodies via optical detection with Cy5-conjugated secondary antibodies (Santa Cruz Biotechnology, USA). In order to accomplish this, n = 8 oxygen-plasma cleaned (15 min at 50 sccm O₂, 200 W, 100 mTorr; Model SE80, Barrel Asher Plasma Technology, USA) borosilicate cover glasses (13-mm-diameter) were placed in the bottom of a sterile 24-well Nunclon Delta S1 Multidish (Nunc, USA). Approximately 1 mL PW medium containing 100 μL of *X. fastidiosa* 9a5c culture (OD$_{600}$ of 0.1) was added to different multidish wells that contain the glass substrates for bacterial adhesion and growth. After bacterial growth for 12 h at 28 °C, the medium was gently removed and samples were washed twice for 5 min each in phosphate-buffered saline (PBS, pH 7.4).

To slightly permeabilize the outer membrane and the peptidoglycan layer of the Gram-negative bacteria, 500 μL of lysozyme (5 mg·mL⁻¹) in PBS was added to the wells and incubated for 60 min, followed by washing of the wells three times with PBS for 3 min each. To reduce

non-specific physisorption of the specific antibodies, 500 μL of bovine serum albumin (BSA; 2%, w/v)-PBS blocking solution was added to each sample well and incubated for 1 h at room temperature. After washing the wells three times with PBS-Tween 20 (0.05% v/v) for 2 min each, the polyclonal anti-XfPal and anti-XfTolB antibodies were added to each sample well at a concentration of 10 μg·mL⁻¹ in PBS-BSA and incubated for 1 h at 37 °C. The samples were then washed three times with PBS-Tween 20 for 2 min each. For fluorescence labeling of the target proteins, 200 μL of PBS-BSA containing 1 μg·mL⁻¹ goat anti-rabbit Cy5-conjugated IgG (Santa Cruz Biotechnology, USA) was added to the samples and incubated for 1 h at 37 °C, protected from light. In a final step, the samples were washed twice for 2 min with PBS-Tween 20, three times with PBS for 3 min and briefly with deionized water and then finally dried gently in a nitrogen stream. The immunolabeling experiments were performed six times for both XfTolB and XfPal detection.

For target protein localization via immunofluorescence labeling, the prepared samples were examined using an epifluorescence microscope (Nikon TE2000U, USA) with a Peltier-cooled back-illuminated EMCCD camera (Andor IXON3, 1024 × 1024 pixels; Galway, Ireland) in combination with an 100× oil-immersion objective (CFI APO TIRF, NA. 1.45, Nikon, USA). Cy5 fluorophore and bacterial autofluorescence excitation was achieved using a 150 W mercury vapor lamp with filter sets (F41-054 and F41-008; AHF, Tübingen, Germany) for green (λ_{ex} = 480 nm) and red (λ_{ex} = 640 nm) light excitation. For each immunolabeled sample, the bacterial autofluorescence in the green wavelength regime (λ_{em} = 550/50 nm) was measured, followed by a measurement in the red emission spectra (λ_{em} = 690/20 nm) for the localization of the Cy5-conjugated secondary antibody. The resulting images (n = 290) were superimposed to identify protein localization in reference to the bacterial shape.

2.6. Analytical size-exclusion chromatography

The interaction between the purified recombinant XfTolB and XfPal proteins was initially evaluated in vitro by analytical size-exclusion chromatography (SEC) with a Superdex 200 10/300 GL prepacked column (GE Healthcare, Uppsala, Sweden) as described by Zhang et al. [17]. Protein samples were dialyzed against 50 mM Tris–Cl pH 8.0 buffer containing 150 mM NaCl and 1 mM CaCl₂ (buffer C), and individual proteins or a mixture of proteins at equal concentrations (~50 mM) was incubated for 15 h at 4 °C. Then, individual XfTolB and XfPal samples and a preincubated isostoichiometric mixture of XfTolB and XfPal were separated on the column, which was previously equilibrated with buffer C, at a flow rate of 0.5 mL·min⁻¹. The elution fractions of each chromatographic run were collected, precipitated with trichloroacetic acid and analyzed by 12% SDS-PAGE.

2.7. Small-angle X-ray scattering

The XfTolB–XfPal complex isolated from analytical SEC experiments was subjected to SAXS. The SAXS data collection was performed at the SAXS-1 beamline at the Brazilian National Synchrotron Light Laboratory (LNLS; Campinas, Brazil) [40] using a Dectris-Pilatus (300 K, 84 mm × 107 mm) 2D detector and a monochromatic X-ray beam with a wavelength of 1.3808 Å. The sample-to-detector distance was adjusted to 1101.504 mm to cover a momentum transfer interval of 0.01585 < q < 0.44263 Å⁻¹, where q = (4π) · (λ)⁻¹ sin θ and 2θ is the scattering angle. XfTolB–XfPal complex samples (~1.5 mg·mL⁻¹) in buffer C were carefully loaded into cells composed of two thin, parallel mica windows. The scattering patterns of the protein samples and buffer solution were measured with a 60–300 s exposure time at 4 °C.

Radial integration of the collected images, correction by sample attenuation and normalization relative to the intensity of the transmitted beam after buffer scattering subtraction were performed using FIT2D

[41]. The SAXS data analyses were performed using the ATSAS software package [42]. The scattering intensity at zero angle I(0) and the Rg were calculated from data with low q values (qRg ≤ 1.3) using the indirect Fourier transform method implemented in GNOM software [43], which also calculates the distance distribution function P(r) and allows the assessment of D_{max} and molecule anisometry. Kratky plots of $q^2I \times q$ [44,45] were also generated to evaluate the conformational variability of the protein in solution. The molecular weight of the protein was estimated using the SAXS Mow algorithm [46].

Ab initio dummy bead models were calculated from the experimental curves using the programs DAMMIN and DAMMIF [47,48]. The final low-resolution three-dimensional envelope, which represents the protein in solution, was generated by averaging independent runs with DAMAVER and DAMFILT software [49]. The individual and averaged SAXS envelopes were visually inspected. The low-resolution envelope from the SAXS experimental curve was superimposed on the available E. coli TolB–Pal complex crystal structure (PDB code 2HQS) [15] using PyMOL (PyMOL Molecular Graphics System, version 1.4.1, Schrödinger, LCC).

The goodness of fit (χ parameter) between the experimental data and the theoretical scattering curves computed for the possible atomic model was assessed using CRYSOL software [50]. Structural alignments were performed using the SUPCOMB software package [51].

3. Results

3.1. Structural X. fastidiosa tol–pal cluster organization and involvement of XfTolB and XfPal in membrane integrity

Initially, we investigated the structure and organization of the tol–pal gene cluster in the X. fastidiosa 9a5c strain genome. The structure of the tol–pal operon is well conserved in Gram-negative bacteria [9]. The X. fastidiosa tol–pal operon (Supplemental Fig. S1) exhibits the same organization and size (approximately 6 kb) as that in E. coli, with the exception of the inclusion of a conserved hypothetical protein downstream of the gene encoding Pal in X. fastidiosa. This position should be occupied by ybgF. However, this conserved hypothetical protein in X. fastidiosa (Xforf_hyp) and YbgF in E. coli (EcYbgF) exhibit 30% amino acid identity (Supplemental Fig. S2). Furthermore, Xforf_hyp contains a peptide signal comprising amino acid residues 1 to 23 (predicted by SignalP4.1 server; http://www.cbs.dtu.dk/services/SignalP/), is a bacterial periplasmic space protein with 0.701 certainty (Psort prediction; http://psort.hgc.jp/form.html) and is predicted to possess tetratricopeptide repeat-like regions (Smart server; http://smart.embl-heidelberg.de/). These structural features are shared by EcYbgF, and based on its chromosome location, this conserved hypothetical protein (Xforf_hyp) is likely YbgF in X. fastidiosa. In addition, similarly as it occurs in E. coli two distinct gene pairs homologous to tolQ and tolR also are present in the available X. fastidiosa 9a5c genome.

Due to the high sequence identity of XfTolB (42%) and XfPal (48%) with their homologs in E. coli, the in vivo functionality of xftolB and xfpal was tested using a complementation assay based on the sensitivity of tolB⁻ and pal⁻ E. coli mutants to the detergent sodium dodecyl sulfate (SDS). The E. coli tolB⁻ and pal⁻ knockout strains were complemented with full-length xftolB and xfpal, respectively, and the inhibitory effect of SDS on wild-type, null mutants and mutants complemented with X. fastidiosa genes (Table 1) was assessed. xftolB and xfpal were able to functionally complement the E. coli mutants (Fig. 1). The wild-type strain (Fig. 1A) did not exhibit any inhibition of cell growth around the diffusion filter disc containing 10% (w/v) SDS in the test performed on BHI plates. By contrast, a clear inhibition zone was observed for the tolB⁻ and pal⁻ mutants (Fig. 1B and C, respectively). However, when these mutants were complemented with xftolB and xfpal under the control of the araCP$_{BAD}$ arabinose-inducible promoter in pBAD24 [36], an inhibitory area was not observed (Fig. 1D and E, respectively); these results were very similar to those observed for the wild-type
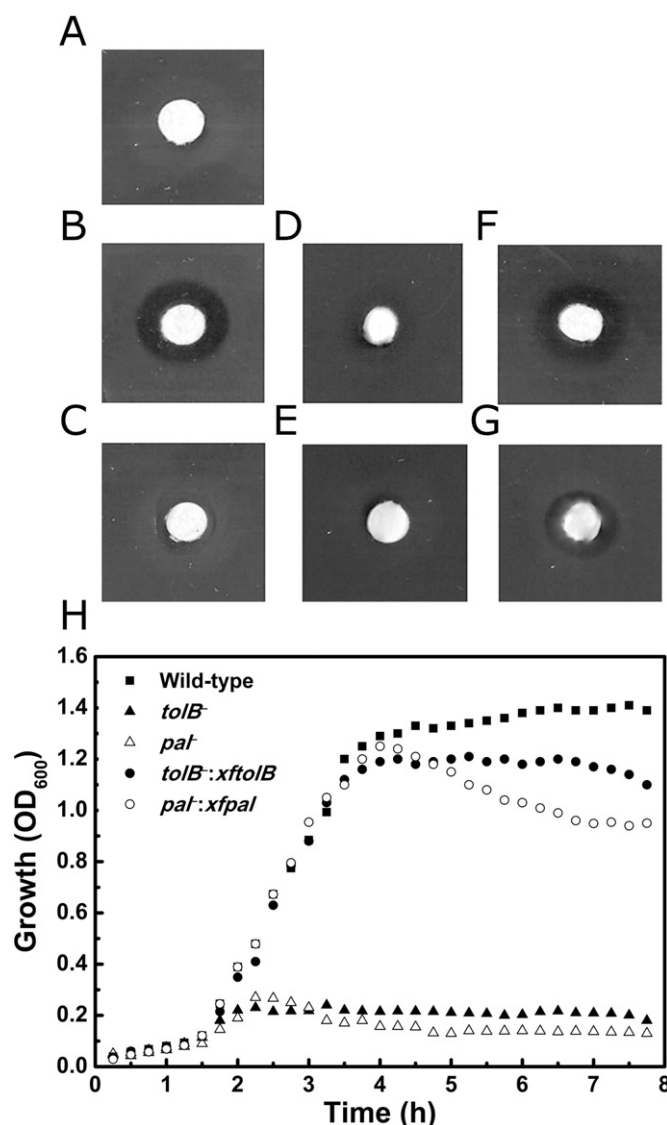
Fig. 1. XfTolB and XfPal are involved in membrane integrity in E. coli cells. Panels A–G show the SDS-associated phenotype in wild-type E. coli and the tolB⁻ and pal⁻ knockout mutants and null mutants complemented with xftolB and xfpal, respectively. (A) The wild-type, (B) tolB⁻, (C) pal⁻, (D) tolB⁻–xftolB, (E) pal⁻–xfpal, (F) tolB⁻–empty pBAD24 and (G) pal⁻–empty pBAD24 strains were inoculated on BHI plates supplemented with 0.2% (w/v) L-arabinose, 30 μg·mL⁻¹ kanamycin (B–G) and 100 μg·mL⁻¹ ampicillin (D–G) at 37 °C. The SDS growth inhibitory effect was assessed using an adapted Kirby–Bauer diffusion test with a 5-mm-diameter filter paper disc with 5 μL of 10% (w/v) SDS. (H) Growth curves of the wild-type, knockout strains and null mutants with xftolB and xfpal in BHI liquid culture in the presence of 0.2% (w/v) SDS. The growth of the bacterial cells was assessed by determining the turbidity (OD$_{600}$) every 15 min for 8 h. All experiments were performed in triplicate.

strain (Fig. 1A). The null mutants were also complemented with the empty vector (pBAD24) used to clone xftolB and xfpal as a negative control for the complementation assays (Fig. 1F and G). Identical results were obtained for the E. coli knockout mutants (Fig. 1B and C), confirming the role of xftolB and xfpal in restoring the SDS-associated phenotype of the mutant strains.

The effect of 0.2% (w/v) SDS on cell growth was also investigated by determining the turbidity (OD$_{600}$) of the wild-type, mutants and mutants complemented with xftolB and xfpal in BHI liquid culture (Fig. 1H). The cell growth of the mutants complemented with xftolB and xfpal was similar to that of wild-type in the presence of SDS, confirming the results obtained on BHI plates (Fig. 1A–G). Not surprisingly, after 4 h of bacterial growth, in the early stationary phase, a decrease in cell growth was observed for mutants in which the tolB or

pal genes were complemented. This characteristic may be associated with a defect in the induction of gene expression by arabinose or protein instability. Nevertheless, the null mutants and mutants complemented with the empty vector were unable to grow in BHI liquid medium at SDS concentrations 50 times lower than those used in tests performed on BHI plates. Therefore, our results confirm the involvement of XfTolB and XfPal in membrane integrity in vivo.

3.2. Detection and determination of the cellular distribution of XfTolB and XfPal during X. fastidiosa growth by immunodetection techniques

Recombinant XfTolB protein with a C-terminal His$_6$-tag was cloned, overexpressed in an *E. coli* expression host and purified in this study. Approximately 25 mg of pure recombinant protein (approximately 95% purity) was obtained per liter of induced bacterial culture. The secondary folding of the purified recombinant protein was determined primarily by circular dichroism analysis. The XfTolB circular dichroism spectrum revealed the presence of a typical secondary structure for a β-barrel protein (Supplemental Fig. S3), as expected for TolB. The XfPal protein was produced as described by Santos et al. [37]. The secondary folding of purified XfPal was assessed by circular dichroism and was consistent with previously reported results [37] (data not shown).

Polyclonal antibodies against XfTolB and XfPal were produced and used for immunodetection of XfTolB and XfPal during *X. fastidiosa* biofilm and planktonic growth and for in vivo immunolabeling *X. fastidiosa* cells to determine the subcellular localization of XfTolB and XfPal (Fig. 2).

We investigated the expression of XfTolB and XfPal between 3 and 30 days of bacterial growth, which comprises the steps from the initial adhesion of the cells to the surface to be colonized to the last step of the biofilm development process, the dispersion phase [38].
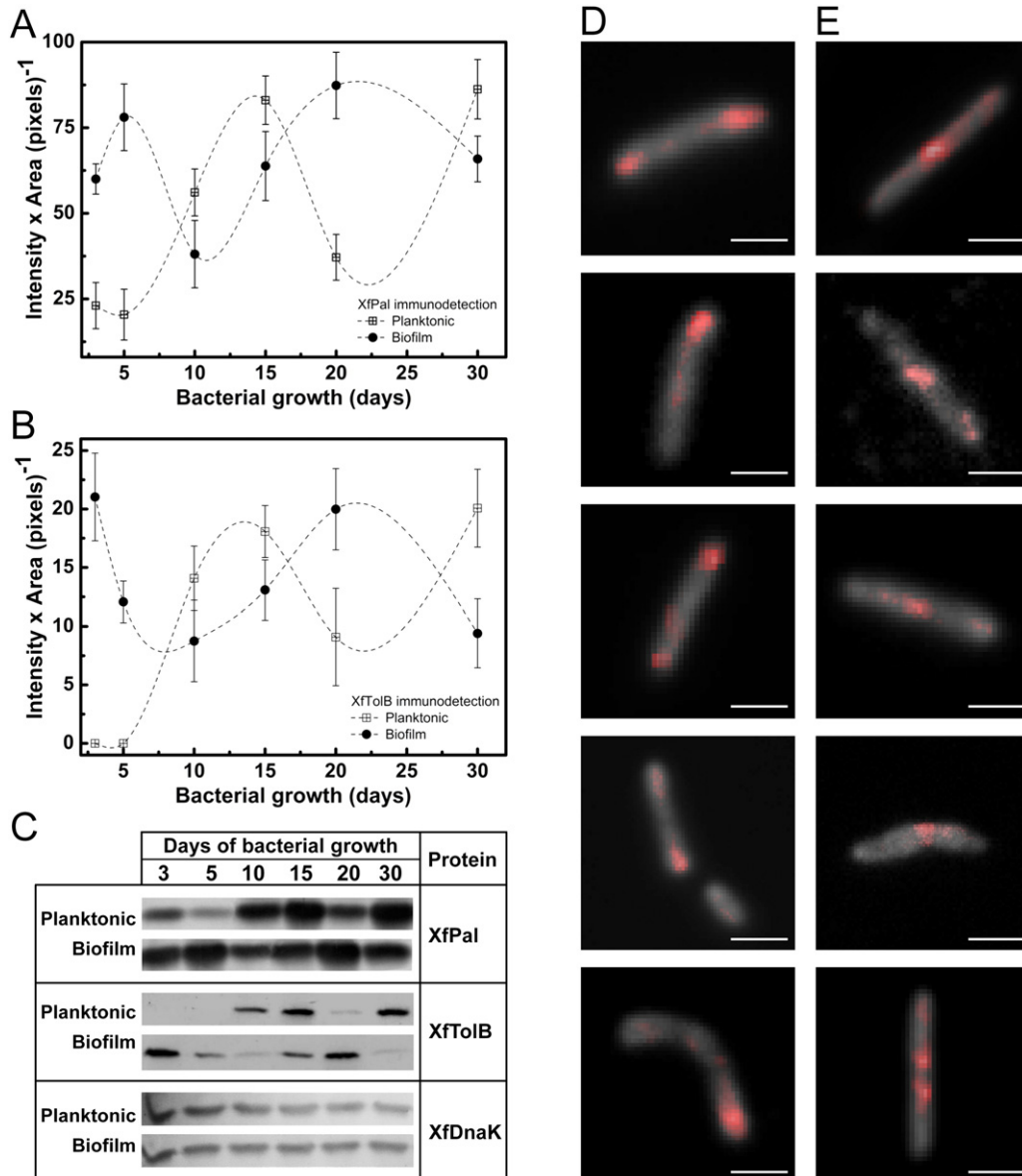
Fig. 2. XfTolB and XfPal immunodetection during *X. fastidiosa* growth. (A) The profiles of XfPal and (B) XfTolB protein expression in biofilm (black circles) and planktonic (open squares) cells collected during *X. fastidiosa* biofilm development were determined by (C) XfPal and XfTolB immunoblotting on nitrocellulose membranes using polyclonal antibodies against XfPal and XfTolB and quantified using EDAS software. The results (A–B) represent the mean of three independent experiments and are presented in a c-spline interpolation. Approximately 5 μg of total *X. fastidiosa* protein from each biofilm developmental phase and planktonic growth was resolved on a 12% SDS-PAGE gel prior to immunodetection experiments. The DnaK protein from *X. fastidiosa* (XfDnaK) was used as a loading control. The error bars indicate the SE of triplicate experiments. (D) Fluorescence based in vivo localization of XfTolB and (E) XfPal proteins in *X. fastidiosa* cells after 12 h of the bacterial growth. For each target protein, n = 5 example images are shown. The bacterial autofluorescence (gray) is superposed with the complementary emission of the Cy5 fluorophore (red) measured using a widefield epifluorescence microscope. Scale bars denote 1 μm.

Immunoblotting of XfPal and XfTolB during *X. fastidiosa* growth in planktonic and biofilm modes (Fig. 2C) demonstrated that XfPal and XfTolB expression differed in these modes. Surprisingly, the expression profiles of XfPal and XfTolB appeared to be dynamic and coordinated (Fig. 2A and B). When the expression of XfTolB or XfPal was high during biofilm growth, its expression was low in the corresponding planktonic condition, and the converse was true when protein expression was high in the planktonic condition. In addition, the expression profiles of XfPal and XfTolB were similar in a specific growth mode of *X. fastidiosa* (Fig. 2A and B). The expression of XfTolB and XfPal was significantly ($P < 0.05$, *t*-test) higher at 3, 5 and 20 days of *X. fastidiosa* biofilm development, which correspond to initial bacterial cell surface adhesion, irreversible adhesion to the surface and mature biofilm, respectively [38].

To visualize the cellular distribution of the XfPal and XfTolB proteins during *X. fastidiosa* growth in vitro, we immunolabeled these proteins and investigated them using fluorescence microscopy. The target XfTolB and XfPal proteins were located at the apical ends of the *X. fastidiosa* cells and/or the center of the bacterial cells (Fig. 2D and E, respectively).

3.3. Characterization and isolation of the recombinant XfTolB–XfPal complex in vitro

By performing analytical SEC experiments, we isolated the XfTolB–XfPal complex in vitro (Fig. 3). Initially, individual samples of XfTolB and XfPal were loaded onto a Superdex 200 10/300 GL column, and the retention time during the chromatographic runs was determined for each sample (Fig. 3A). XfTolB was eluted as a unique peak during analytical SEC assays, while XfPal exhibited two peaks, one corresponding to an apparent monomeric form and the other resembling a large oligomer. The XfPal SEC profile is justified by the fact that the protein was produced using a refolding protocol and/or intrinsic protein properties, as previously reported [37].

The preincubated isostoichiometric mixture of XfTolB and XfPal was subjected to separation by SEC. We observed the following (Fig. 3A): (i) a decrease in the peak corresponding to XfTolB (Fig. 3A — peak 1); (ii) a disappearance of the peak corresponding to the monomeric XfPal fraction (Fig. 3A — peak 2); and (iii) the appearance of an additional peak that does not match any other peak obtained in the analysis of the individual samples (Fig. 3A — peak 3). Fractions collected at the center peaks of the individual XfTolB (Fig. 3A — peak 1) and XfPal (Fig. 3A — peak 2) samples and the additional peak formed by the XfTolB–XfPal mixture (Fig. 3A — peak 3) observed in the chromatographic runs were analyzed by SDS-PAGE, which revealed that the additional peak formed in the XfTolB and XfPal sample (Fig. 3A — peak 3) represents the retention time of the XfTolB–XfPal complex in solution (Fig. 3B).

An additional chromatographic run of the sample collected from the additional peak observed in the XfTolB and XfPal mixture was conducted to isolate the complex and evaluate its stability. The collected XfTolB–XfPal complex was eluted as a unique peak during the new chromatographic run (Fig. 3C), and the presence of unbound individual XfTolB and XfPal or aggregate protein samples was not observed. Thus, the XfTolB–XfPal complex was isolated in vitro and is stably maintained in solution (Fig. 3C and D).

3.4. Overall features of the structural model of the XfTolB–XfPal complex in solution

We performed SAXS experiments to obtain a low-resolution structure of the XfTolB–XfPal complex in solution. The SAXS scattering curves for the XfTolB–XfPal complex isolated by SEC are shown in Fig. 4A.
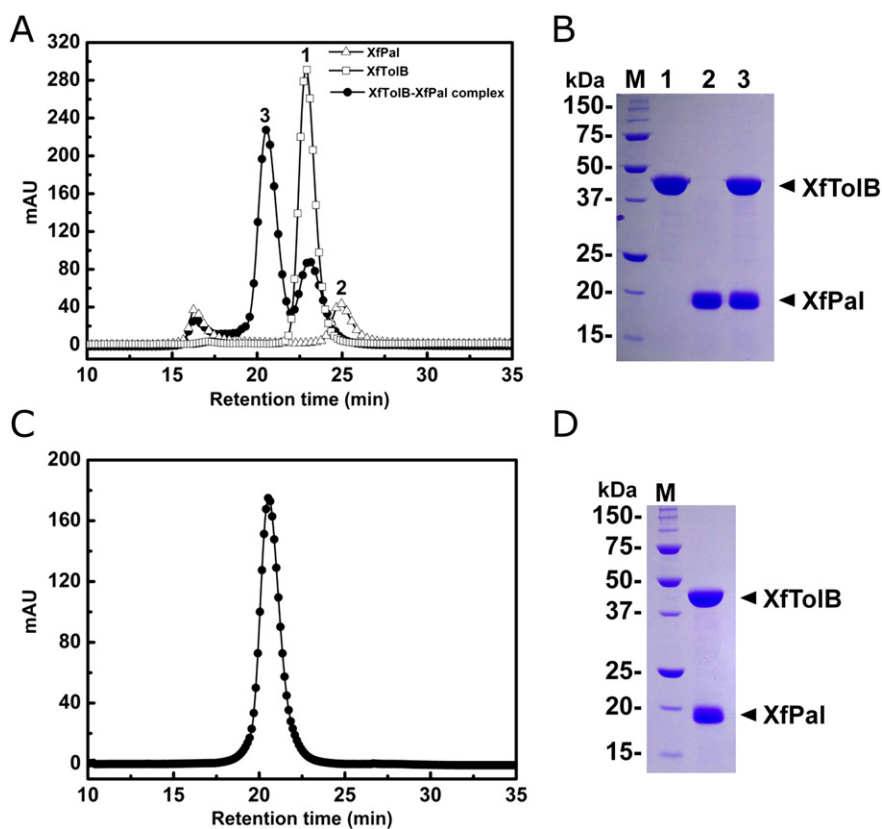
Fig. 3. Detection and isolation of the XfTolB–XfPal complex by analytical SEC. (A) Chromatographic runs of the individual XfTolB and XfPal samples and the preincubated isostoichiometric mixture of XfTolB and XfPal. (B) Fractions collected at center peaks 1–3 of the XfTolB, XfPal or XfTolB–XfPal complex retention profiles in panel A were precipitated with trichloroacetic acid and analyzed by SDS-PAGE. (C) Additional chromatographic separation of the collected central peak attributed to the XfTolB–XfPal complex (peak 3, panel A). (D) SDS-PAGE analysis of the collected peak of the XfTolB–XfPal complex in panel C. All chromatographic runs were performed using a Superdex 200 10/300 GL prepacked column at a flow rate of 0.5 mL·min^{-1}.
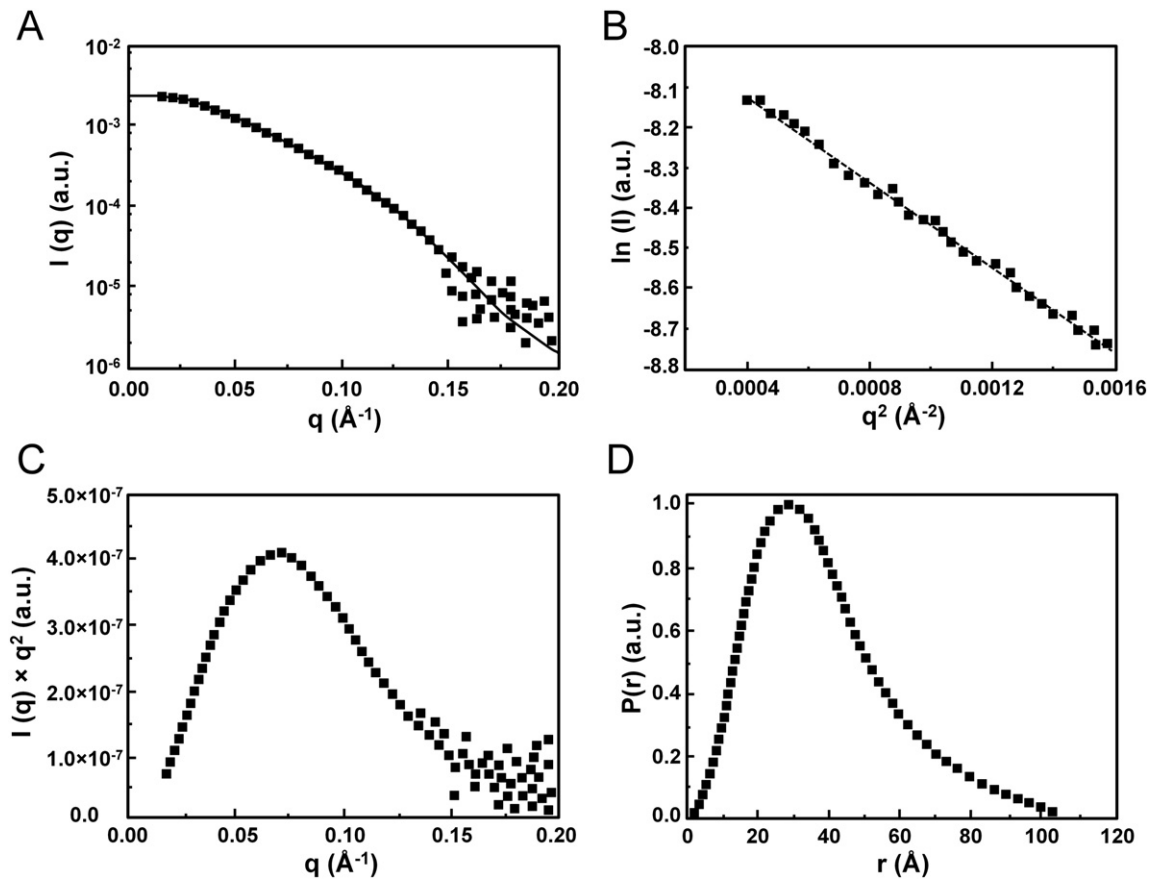
Fig. 4. SAXS analysis of the XfTolB–XfPal complex in solution. (A) XfTolB–XfPal complex scattering curve. The solid line corresponds to the fitting of the theoretical curve calculated for the envelope by computational methods. A χ value of 1.79 was obtained with CRYSOL up to a $q_{max} = 0.2$, as shown in the plot. (B) Linear fitting obtained from Guinier analysis. (C) Kratky plot derived from the experimental curves and normalized for I(0) = 1. (D) The distance distribution function P(r) calculated from the experimental curves was used for ab initio envelope modeling; the higher peak to the left of the center of the range indicates that the XfTolB–XfPal complex exhibits a prolate shape. Negative intensity points in the Kratky plots at higher q values due to the low sample concentration were subtracted. The plot is limited to the region $Iq^2 > 0$.

Because of the low sample concentration (approximately 1.5 mg·mL^{-1}), which was a result of the analytical method used to separate the complex, noisier scattering curves were observed at higher angles (q > 0.15 Å^{-1}). However, the linear behavior of the Guinier plot confirmed the data quality and sample monodispersity, which are essential for SAXS data analysis. Five scattering frames with increasing exposure time (60–300 s) were collected, and the SAXS data presented here (Fig. 4A) represent the average of the collected curves because all curves exhibited the same scattering pattern. The XfTolB–XfPal complex Guinier region is displayed in Fig. 4B. The radius of gyration (Rg) calculated from the linear regression in the Guinier plot was 29.6 Å. The Kratky plot was also evaluated (Fig. 4C) and revealed a typical well-defined maximum for a compact and correctly folded protein. The molecular mass of the complex in solution was estimated as 66.3 ± 3 kDa by SAXS Mow software [46]. The estimated molecular weight obtained from SAXS data is consistent with the expected sum of the molecular masses of recombinant His$_6$-tag protein XfTolB (monomer mass, 46 kDa) and XfPal (monomer mass, 18 kDa) and confirms that the stoichiometry of the interaction between TolB and Pal is 1:1. The XfTolB–XfPal complex distance distribution function P(r) revealed a maximum intramolecular distance (D$_{max}$) of 100 Å (Fig. 4D). However, the distance peak was concentrated at short distances, which indicates a prolate structure. Furthermore, using the indirect Fourier transform implemented in GNOM [43], the Rg from the P(r) was more accurately estimated as 30.1 Å, which is consistent with the values obtained in the Guinier analysis.

The structural model of the XfTolB–XfPal complex in solution recovered from the scattering curves is shown in Fig. 5. This envelope was superimposed onto the E. coli TolB–Pal complex crystal structure (PDB code 2HQS) [15], revealing a remarkable fit. The excellent fit and correctness of the atomic model (Fig. 4A) were confirmed by the chi-square value of 1.79 obtained for the comparison of the experimental SAXS curves and the theoretical scattering curves computed for the XfTolB–XfPal envelope.

4. Discussion

The data presented in this study reveal a dynamic, coordinated expression profile for XfTolB and XfPal during X. fastidiosa biofilm growth. We also confirmed the in vivo involvement of XfTolB and XfPal in membrane integrity using E. coli mutants and demonstrate its cellular localization by fluorescence microscopy. In addition, we isolated the XfTolB–XfPal complex in solution and determined its low-resolution structure for the first time.

Although the fine details of the physiological function of the proteins encoded by the tol–pal cluster are not fully understood, its role in the virulence of several bacteria is increasingly recognized [22–28,30]. The role of the Tol–Pal system in maintaining cell envelope integrity [5,6] appears to be conserved in X. fastidiosa, as demonstrated by the ability of xftolB and xfpal to restore an SDS-associated phenotype in the E. coli tolB$^-$ and pal$^-$ knockout strains, respectively.

During evolution, bacteria appear to have selected a wide range of macromolecules related to the architecture and diversity of the cell envelope structure [52–54]. In particular, those proteins involved in membrane integrity that are able to maintain a cohesive and stable bacterial shape, e.g., the Tol–Pal components, and consequently promote the effective colonization of a habitat directly reflect the microbial
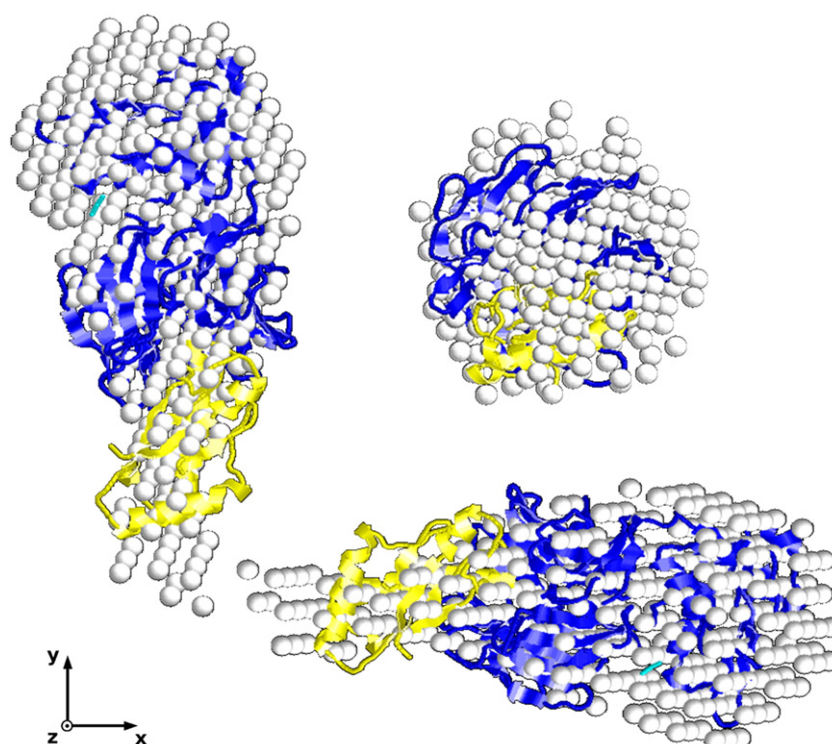
Fig. 5. Structural model of the XfTolB–XfPal complex in solution recovered from the SAXS data analysis. The experimental SAXS data were superimposed onto the atomic model of the *E. coli* TolB/Pal complex crystal structure (PDB code 2HQS), revealing a remarkable fit. The middle and bottom views are rotated 90° clockwise around the y- and x-axes, respectively. TolB and Pal from the atomic structure of the *E. coli* TolB/Pal complex are highlighted in blue and yellow, respectively. The figures were generated using PyMOL (Schrodinger LLC), and additional edits were performed using GIMP 2.8 software (http://www.gimp.org/).

plasticity in response to a broad spectrum of selective pressures in the environment, including ionic strength and osmolarity. Thereby, our findings indicate that both XfTolB and XfPal may play a variety of protective and adaptive roles.

Differences in gene expression profiles and metabolomics associated with bacterial growth in biofilm or planktonic mode, including *P. aeruginosa*, *Pseudomonas fluorescens* and *X. fastidiosa*, have been reported [28,38,39,55–58]. The temporal expression profile of the *tol–pal* mRNAs during the cell division cycle of *Caulobacter crescentus* indicates that *tolQ*, *tolR*, *tolA* and *tolB* expressions are not regulated by the cell cycle [59]. Although high *pal* transcript levels are observed in *C. crescentus* swarmer cells, Pal protein levels do not exhibit significant changes during the course of the cell cycle [59]. Herein, we report that XfTolB and XfPal are differentially expressed and exhibit a dynamic, coordinated expression pattern during the biofilm and planktonic modes of *X. fastidiosa* growth. The expression level of XfPal as assayed by immunodetection with an anti-XfPal antibody was considerably higher than that observed in the XfTolB analyses. However, studies of fractionation and quantification focusing on the Tol–Pal components demonstrated that Pal is present at approximately 2000 to 3000 molecules per μm^2 of cell surface area, corresponding to 8000 to 40,000 copies of Pal per cell, depending on cell morphology [60]. These results indicate that Pal plays a major role in outer membrane integrity [5,6,11,60]. Our findings indicate that XfTolB and XfPal are important in the early stages of bacterial biofilm development; high amounts of protein were also detected in the mature biofilm phase. The early stages of *X. fastidiosa* biofilm formation are marked by the expression of proteins involved in substrate adhesion [3,56], and thus the stability of the cell envelope appears to have a direct impact on the ability of a bacterium to colonize a particular host, explaining the expression of the Tol–Pal system in these stages of biofilm development. During the mature biofilm phase, the growth of the bacterial community is coordinated and is at its highest level; thus, the high expression of XfTolB and

XfPal is not surprising, particularly as the Tol–Pal system may be involved in the cell division machinery.

The immunofluorescence experiments suggested that XfTolB and XfPal can occupy the same subcellular localization during *X. fastidiosa* growth. Interestingly, by green fluorescent protein fusion, the five proteins of the Tol–Pal system (TolQ, TolR, TolA, TolB and Pal) have been demonstrated to accumulate at cell constriction sites in *E. coli* [21]. In the *Caulobacter* Tol–Pal complex, cryoelectron microscopy images of *tolA-*, *tolB-* and *pal*-depleted mutants revealed that the cells failed to complete cell division, highlighting the role of the proteins in this complex in mediating outer membrane constriction at the last step of cell division and positioning a protein localization factor [59]. Thus, the visualization of XfTolB and XfPal at the poles and in the center of the cell suggests that these proteins are involved in the replication of *X. fastidiosa*. However, from the immunolabeling data, we cannot confirm conclusively that these proteins accumulate at the cell division plane in *X. fastidiosa*. Nevertheless, this is a valuable observation as it was already reported for some biofilm-forming bacteria as *Klebsiella pneumoniae* that the attachment to the substrate occurs at the poles of the cells [61].

Physical contact between the proteins of the Tol–Pal system is controversial. An initial study indicated an interaction between Pal and TolA in vivo [62]. However, a subsequent study was unable to detect any interaction between the two proteins in vitro [63]. By contrast, an in vitro and in vivo interaction between TolB and Pal was detected early [12,13]. The crystallographic structure of the TolB–Pal complex from *Yersinia pestis* (PDB code 4R40) and *E. coli* is available (PDB code 2HQS) [15], and we isolated and elucidated the low-resolution structure of the *X. fastidiosa* XfTolB–XfPal complex in solution by SAXS. SAXS is a promising technique to study proteins in solution because it enables analysis under physiological conditions similar to those in which the proteins act in vivo and permits the study of protein–protein interactions. The XfTolB–XfPal is a highly stable protein–protein complex that

exhibits a prolate structure in solution. Interestingly, TolB possesses a distinct two-domain structure comprising an N-terminal mixed α/β domain and a C-terminal six-bladed β-propeller domain [64], while Pal comprises a four-stranded mixed β-sheet and four α-helices [15]. Pal binds within the bowl formed by connecting strands of the propeller blades at the C-terminal domain of TolB, yielding a prolate structure with a unit cell length of a = 74.85 Å, b = 89.05 Å and c = 91.05 Å [15]. While the XfTolB–XfPal complex in solution exhibits a configuration similar to that of the 2HQS structure, the former exhibited a D_{max} of 100 Å. Thus, the global rearrangement of TolB and Pal for protein–protein binding may be more flexible in vivo and affect the ability of TolB to associate with other proteins in the outer membrane and periplasm and the ability of Pal to bind to the peptidoglycan layer.

Although attempts to construct *X. fastidiosa* 9a5c mutants have not been successful [65,66], partly due to poor growth in classical rich medium, future studies focusing on the inactivation of the *tol–pal* gene cluster will provide new information regarding the role of these genes during bacteria–plant infection, particularly given the modulation of host colonization by the blocking of surface attachment by *X. fastidiosa* outer membrane vesicles [67]. Furthermore, because XfTolB and XfPal are involved in membrane integrity and exhibit a dynamic, coordinated expression profile during the major phases of bacterial biofilm establishment, these proteins are important targets for the control of the biofilm development process.

Conflict of interest

The authors have declared that no competing interests exist.

Acknowledgements

Appendix A. Supplementary data

Supplementary data to this article can be found online at http://dx.doi.org/10.1016/j.bbapap.2015.05.018.

References

[1] T.R. Garrett, M. Bhakoo, Z. Zhang, Bacterial adhesion and biofilms on surfaces, Prog. Nat. Sci. 18 (2008) 1049–1056.
[2] C. Chagnot, M.A. Zorgani, T. Astruc, M. Desvaux, Proteinaceous determinants of surface colonization in bacteria: bacterial adhesion and biofilm formation from a protein secretion perspective, Front. Microbiol. 4 (2013) 00303.
[3] H. Feil, W.S. Feil, S.E. Lindow, Contribution of fimbrial and afimbrial adhesins of *Xylella fastidiosa* to attachment to surfaces and virulence to grape, Phytopathology 97 (2007) 318–324.
[4] K. Bazaka, R.J. Crawford, E.L. Nazarenko, E.P. Ivanova, Bacterial extracellular polysaccharides, Adv. Exp. Med. Biol. 715 (2011) 213–226.
[5] J.C. Lazzaroni, P. Germon, M.-C. Ray, A. Vianney, The Tol proteins of *Escherichia coli* and their involvement in the uptake of biomolecules and outer membrane stability, FEMS Microbiol. Lett. 177 (1999) 191–197.
[6] R. Lloubes, E. Cascales, A. Walburger, E. Bouveret, C. Lazdunski, A. Bernadac, L. Journet, The Tol–Pal proteins of the *Escherichia coli* cell envelope: an energized system required for outer membrane integrity? Res. Microbiol. 152 (2001) 523–529.
[7] A. Vianney, M.M. Muller, T. Clavel, J.C. Lazzaroni, R. Portalier, R.E. Webster, Characterization of the tol-pal region of *Escherichia coli* K-12: translational control of *tolR* expression by TolQ and identification of a new open reading frame downstream of *pal* encoding a periplasmic protein, J. Bacteriol. 178 (1996) 4031–4038.
[8] M.M. Muller, R.E. Webster, Characterization of the *tol–pal* and *cyd* region of *Escherichia coli* K-12: transcript analysis and identification of two new proteins encoded by the *cyd* operon, J. Bacteriol. 179 (1997) 2077–2080.
[9] J.N. Sturgis, Organisation and evolution of the *tol–pal* gene cluster, J. Mol. Microbiol. Biotechnol. 3 (2001) 113–122.
[10] R. Koebnik, Proposal for a peptidoglycan-associating alpha-helical motif in the C-terminal regions of some bacterial cell-surface proteins, Mol. Microbiol. 16 (1995) 1269–1270.
[11] R. Godlewska, K. Wisniewska, Z. Pietras, E.K. Jagusztyn-Krynicka, Peptidoglycan-associated lipoprotein (Pal) of Gram-negative bacteria: function, structure, role in pathogenesis and potential application in immunoprophylaxis, FEMS Microbiol. Lett. 298 (2009) 1–11.
[12] E. Bouveret, R. Derouiche, A. Rigal, R. Lloubes, C. Lazdunski, H. Benedetti, Peptidoglycan-associated lipoprotein–TolB interaction. A possible key to explaining the formation of contact sites between the inner and outer membranes of *Escherichia coli*, J. Biol. Chem. 270 (1995) 11071–11077.
[13] E. Bouveret, H. Bénédetti, A. Rigal, E. Loret, C. Lazdunski, *In vitro* characterization of peptidoglycan-associated lipoprotein (PAL)–peptidoglycan and PAL–TolB interactions, J. Bacteriol. 181 (1999) 6306–6311.
[14] M.-C. Ray, P. Germon, A. Vianney, R. Portalier, J.C. Lazzaroni, Identification by genetic suppression of *Escherichia coli* TolB residues important for TolB–Pal interaction, J. Bacteriol. 182 (2000) 821–824.
[15] D.A. Bonsor, I. Grishkovskaya, E.J. Dodson, C. Kleanthous, Molecular mimicry enables competitive recruitment by a natively disordered protein, J. Am. Chem. Soc. 129 (2007) 4800–4807.
[16] R.E. Webster, The *tol* gene products and the import of macromolecules into *Escherichia coli*, Mol. Microbiol. 5 (1991) 1005–1011.
[17] Y. Zhang, C. Li, M.N. Vankemmelbeke, P. Bardelang, M. Paoli, C.N. Penfold, R. James, The crystal structure of the TolB box of colicin A in complex with TolB reveals important differences in the recruitment of the common TolB translocation portal used by group A colicins, Mol. Microbiol. 75 (2010) 623–636.
[18] C. Kleanthous, Swimming against the tide: progress and challenges in our understanding of colicin translocation, Nat. Rev. Microbiol. 8 (2010) 843–848.
[19] M.A. Llamas, J.L. Ramos, J.J. Rodríguez-Herva, Mutations in each of the tol genes of *Pseudomonas putida* reveal that they are critical for maintenance of outer membrane stability, J. Bacteriol. 182 (2000) 4764–4772.
[20] E.D. Vinés, C.L. Marolda, A. Balachandran, M.A. Valvano, Defective O-antigen polymerization in *tolA* and *pal* mutants of *Escherichia coli* in response to extracytoplasmic stress, J. Bacteriol. 187 (2005) 3359–3368.
[21] M.A. Gerding, Y. Ogata, N.D. Pecora, H. Niki, P.A.J. De Boer, The trans-envelope Tol–Pal complex is part of the cell division machinery and required for proper outer-membrane invagination during cell constriction in *E. coli*, Mol. Microbiol. 63 (2007) 1008–1025.
[22] A.J. Heilpern, M.K. Waldor, CTXphi infection of *Vibrio cholerae* requires the *tolQRA* gene products, J. Bacteriol. 182 (2000) 1739–1747.
[23] R. Tamayo, S.S. Ryan, A.J. McCoy, J.S. Gunn, Identification and genetic characterization of PmrA-regulated genes and genes involved in polymyxin B resistance in *Salmonella enterica* serovar *typhimurium*, Infect. Immun. 70 (2002) 6770–6778.
[24] J.F. Dubuisson, A. Vianney, N. Hugouvieux-Cotte-Pattat, J.C. Lazzaroni, Tol-Pal proteins are critical cell envelope components of *Erwinia chrysanthemi* affecting cell morphology and virulence, Microbiology 151 (2005) 3337–3347.
[25] S. Bhatt, C.L. Weingart, Identification of sodium chloride-regulated genes in *Burkholderia cenocepacia*, Curr. Microbiol. 56 (2008) 418–422.
[26] D.E. Cameron, J.M. Urbach, J.J. Mekalanos, A defined transposon mutant library and its use in identifying motility genes in *Vibrio cholerae*, Proc. Natl. Acad. Sci. U. S. A. 105 (2008) 8736–8741.
[27] A. Lo Sciuto, R. Fernandez-Pinar, L. Bertuccini, F. Iosi, F. Superti, F. Imperi, The periplasmic protein TolB as a potential drug target in *Pseudomonas aeruginosa*, PLoS One 9 (2014) e103784.
[28] M. Whiteley, M.G. Bangera, R.E. Bumgarner, M.R. Parsek, G.M. Teitzel, S. Lory, E.P. Greenberg, Gene expression in *Pseudomonas aeruginosa* biofilms, Nature 413 (2001) 860–864.
[29] S.L. Black, A. Dawson, F.B. Ward, R.J. Allen, Genes required for growth at high hydrostatic pressure in *Escherichia coli* K-12 identified by genome-wide screening, PLoS One 8 (2013) e73995.
[30] E. Watson, M.P. Alberdi, N.F. Inglis, A. Lainson, M.E. Porter, E. Manson, L. Imrie, K. McLean, D.G.E. Smith, Proteomic analysis of *Lawsonia intracellularis* reveals expression of outer membrane proteins during infection, Vet. Microbiol. 174 (2014) 448–455.
[31] N.W. Schaad, E. Postnikova, G. Lacy, M. Fatmi, C.J. Chang, *Xylella fastidiosa* subspecies: *X. fastidiosa* subsp. [correction] *fastidiosa* [correction] subsp. nov., *X. fastidiosa* subsp. *multiplex* subsp. nov., and *X. fastidiosa* subsp. *pauca* subsp. nov, Syst. Appl. Microbiol. 27 (2004) 290–300.
[32] K.A. Datsenko, B.L. Wanner, One-step inactivation of chromosomal genes in *Escherichia coli* K-12 using PCR products, Proc. Natl. Acad. Sci. U. S. A. 97 (2000) 6640–6645.
[33] T. Baba, T. Ara, M. Hasegawa, Y. Takai, Y. Okumura, M. Baba, K.A. Datsenko, M. Tomita, B.L. Wanner, H. Mori, Construction of *Escherichia coli* K-12 in-frame, single-gene knockout mutants: the Keio collection, Mol. Syst. Biol. 2 (2006) 2006.0008.
[34] M. Davis, W. French, N. Schaad, Axenic culture of the bacteria associated with phony disease of peach and plum leaf scald, Curr. Microbiol. 6 (1981) 309–314.
[35] J. Sambrook, D.W. Russell, Molecular Cloning: A Laboratory Manual, 3rd ed. Cold Spring Harbor Laboratory, Cold Spring Harbor, 2001. (Place Published).

[36] L.M. Guzman, D. Belin, M.J. Carson, J. Beckwith, Tight regulation, modulation, and high-level expression by vectors containing the arabinose P$_{BAD}$ promoter, J. Bacteriol. 177 (1995) 4121–4130.

[37] C.A. Santos, L.L. Beloti, M.A. Toledo, A. Crucello, M.T. Favaro, J.S. Mendes, A.S. Santiago, A.R. Azzoni, A.P. Souza, A novel protein refolding protocol for the solubilization and purification of recombinant peptidoglycan-associated lipoprotein from *Xylella fastidiosa* overexpressed in *Escherichia coli*, Protein Expr. Purif. 82 (2012) 284–289.

[38] A.A. de Souza, M.A. Takita, H.C.D. Coletta-Filho, C. Caldana, G.M. Yanai, N.H. Muto, R.C. de Oliveira, L.R. Nunes, M.A. Machado, Gene expression profile of the plant pathogen *Xylella fastidiosa* during biofilm formation *in vitro*, FEMS Microbiol. Lett. 237 (2004) 341–353.

[39] C.A. Santos, M.A. Toledo, D.B. Trivella, L.L. Beloti, D.R. Schneider, A.M. Saraiva, A. Crucello, A.R. Azzoni, A.A. Souza, R. Aparicio, A.P. Souza, Functional and structural studies of the disulfide isomerase DsbC from the plant pathogen *Xylella fastidiosa* reveals a redox-dependent oligomeric modulation *in vitro*, FEBS J. 279 (2012) 3828–3843.

[40] G. Kellermann, F. Vicentin, E. Tamura, M. Rocha, H. Tolentino, A. Barbosa, A. Craievich, I. Torriani, The small-angle X-ray scattering beamline of the Brazilian synchrotron light laboratory, J. Appl. Crystallogr. 30 (1997) 880–883.

[41] A.P. Hammersley, S.O. Svensson, M. Hanfland, A.N. Fitch, D. Hausermann, Two-dimensional detector software: from real detector to idealised image or two-theta scan, High Pressure Res. 14 (1996) 235–248.

[42] P.V. Konarev, V.V. Volkov, M.V. Petoukhov, D.I. Svergun, *ATSAS* 2.1, a program package for small-angle scattering data analysis, J. Appl. Crystallogr. 39 (2006) 277–286.

[43] D. Svergun, Determination of the regularization parameter in indirect-transform methods using perceptual criteria, J. Appl. Crystallogr. 25 (1992) 495–503.

[44] S. Doniach, Changes in biomolecular conformation seen by small angle X-ray scattering, Chem. Rev. 101 (2001) 1763–1778.

[45] R.P. Rambo, J.A. Tainer, Characterizing flexible and intrinsically unstructured biological macromolecules by SAS using the Porod–Debye law, Biopolymers 95 (2011) 559–571.

[46] H. Fischer, M. de Oliveira Neto, H.B. Napolitano, I. Polikarpov, A.F. Craievich, Determination of the molecular weight of proteins in solution from a single small-angle X-ray scattering measurement on a relative scale, J. Appl. Crystallogr. 43 (2010) 101–109.

[47] D.I. Svergun, Restoring low resolution structure of biological macromolecules from solution scattering using simulated annealing, Biophys. J. 76 (1999) 2879–2886.

[48] D. Franke, D.I. Svergun, *DAMMIF*, a program for rapid ab-initio shape determination in small-angle scattering, J. Appl. Crystallogr. 42 (2009) 342–346.

[49] V.V. Volkov, D.I. Svergun, Uniqueness of *ab initio* shape determination in small-angle scattering, J. Appl. Crystallogr. 36 (2003) 860–864.

[50] D. Svergun, C. Barberato, M.H.J. Koch, *CRYSOL* — a program to evaluate X-ray solution scattering of biological macromolecules from atomic coordinates, J. Appl. Crystallogr. 28 (1995) 768–773.

[51] M.B. Kozin, D.I. Svergun, Automated matching of high- and low-resolution structural models, J. Appl. Crystallogr. 34 (2001) 33–41.

[52] T.J. Silhavy, D. Kahne, S. Walker, The bacterial cell envelope, Cold Spring Harb. Perspect. Biol. 2 (2010) a000414.

[53] I.C. Sutcliffe, A phylum level perspective on bacterial cell envelope architecture, Trends Microbiol. 18 (2010) 464–470.

[54] P. Messner, C. Schaffer, P. Kosma, Bacterial cell-envelope glycoconjugates, Adv. Carbohydr. Chem. Biochem. 69 (2013) 209–272.

[55] E.L. Gjersing, J.L. Herberg, J. Horn, C.M. Schaldach, R.S. Maxwell, NMR metabolomics of planktonic and biofilm modes of growth in *Pseudomonas aeruginosa*, Anal. Chem. 79 (2007) 8037–8045.

[56] R. Caserta, M.A. Takita, M.L. Targon, L.K. Rosselli-Murai, A.P. de Souza, L. Peroni, D.R. Stach-Machado, A. Andrade, C.A. Labate, E.W. Kitajima, M.A. Machado, A.A. de Souza, Expression of *Xylella fastidiosa* fimbrial and afimbrial proteins during biofilm formation, Appl. Environ. Microbiol. 76 (2010) 4250–4259.

[57] S.C. Booth, M.L. Workentine, J. Wen, R. Shaykhutdinov, H.J. Vogel, H. Ceri, R.J. Turner, A.M. Weljie, Differences in metabolism between the biofilm and planktonic response to metal stress, J. Proteome Res. 10 (2011) 3190–3199.

[58] M.A. Toledo, C.A. Santos, J.S. Mendes, A.C. Pelloso, L.L. Beloti, A. Crucello, M.T. Favaro, A.S. Santiago, D.R. Schneider, A.M. Saraiva, D.R. Stach-Machado, A.A. Souza, D.B. Trivella, R. Aparicio, L. Tasic, A.R. Azzoni, A.P. Souza, Small-angle X-ray scattering and *in silico* modeling approaches for the accurate functional annotation of an LysR-type transcriptional regulator, Biochim. Biophys. Acta 1834 (2013) 697–707.

[59] Y.C. Yeh, L.R. Comolli, K.H. Downing, L. Shapiro, H.H. McAdams, The *Caulobacter* Tol–Pal complex is essential for outer membrane integrity and the positioning of a polar localization factor, J. Bacteriol. 192 (2010) 4847–4858.

[60] E. Cascales, A. Bernadac, M. Gavioli, J.C. Lazzaroni, R. Lloubes, Pal lipoprotein of *Escherichia coli* plays a major role in outer membrane integrity, J. Bacteriol. 184 (2002) 754–759.

[61] D. Balestrino, J.-M. Ghigo, N. Charbonnel, J.A.J. Haagensen, C. Forestier, The characterization of functions involved in the establishment and maturation of *Klebsiella pneumoniae in vitro* biofilm reveals dual roles for surface exopolysaccharides, Environ. Microbiol. 10 (2008) 685–701.

[62] E. Cascales, M. Gavioli, J.N. Sturgis, R. Lloubes, Proton motive force drives the interaction of the inner membrane TolA and outer membrane Pal proteins in *Escherichia coli*, Mol. Microbiol. 38 (2000) 904–915.

[63] D.A. Bonsor, O. Hecht, M. Vankemmelbeke, A. Sharma, A.M. Krachler, N.G. Housden, K.J. Lilly, R. James, G.R. Moore, C. Kleanthous, Allosteric β-propeller signalling in TolB and its manipulation by translocating colicins, EMBO J. 28 (2009) 2846–2857.

[64] C. Abergel, E. Bouveret, J.M. Claverie, K. Brown, A. Rigal, C. Lazdunski, H. Benedetti, Structure of the *Escherichia coli* TolB protein determined by MAD methods at 1.95 Å resolution, Structure 7 (1999) 1291–1300.

[65] P. Gaurivaud, L.C.A. Souza, A.C.D. Virgílio, A.G. Mariano, R.R. Palma, P.B. Monteiro, Gene disruption by homologous recombination in the *Xylella fastidiosa* citrus variegated chlorosis strain, Appl. Environ. Microbiol. 68 (2002) 4658–4665.

[66] C. Teixeira Ddo, S.R. Rocha, M.A. de Santos, A.G. Mariano, W.B. Li, P.B. Monteiro, A suitable *Xylella fastidiosa* CVC strain for post-genome studies, Curr. Microbiol. 49 (2004) 396–399.

[67] M. Ionescu, P.A. Zaini, C. Baccari, S. Tran, A.M. da Silva, S.E. Lindow, *Xylella fastidiosa* outer membrane vesicles modulate plant colonization by blocking attachment to surfaces, Proc. Natl. Acad. Sci. U. S. A. 111 (2014) E3910–E3918.

Characterization of the TolB-Pal trans-envelope complex from *Xylella fastidiosa* reveals a dynamic and coordinated protein expression profile during the biofilm development process

Clelton A. Santos[a], Richard Janissen[b1], Marcelo A. S. Toledo[a], Lilian L. Beloti[a], Adriano R. Azzoni[c], Monica A. Cotta[b], Anete P. Souza[a,d,*]

[a]*Centro de Biologia Molecular e Engenharia Genética, Universidade Estadual de Campinas, Campinas, SP, Brazil*
[b]*Instituto de Fisica Gleb Wataghin, Universidade Estadual de Campinas, Campinas, SP, Brazil*
[c]*Departamento de Engenharia Química, Escola Politécnica, Universidade de São Paulo, São Paulo, SP, Brazil*
[d]*Departamento de Biologia Vegetal, Instituto de Biologia, Universidade Estadual de Campinas, Campinas, SP, Brazil*
[#a]*Current Address: Kavli Institute of Nanoscience, Delft University of Technology, Lorentzweg 1, Delft, The Netherlands*

Supplementary Figures S1-S3

*Address correspondence to: Anete P. Souza, Centro de Biologia Molecular e Engenharia Genética (CBMEG), Universidade Estadual de Campinas, Rua Candido Rondon 400, Cidade Universitária "Zeferino Vaz", CP 6010, 13083-875, Campinas, São Paulo, Brazil, Tel. and Fax: +55 19 3521-1089; E-mail: anete@unicamp.br
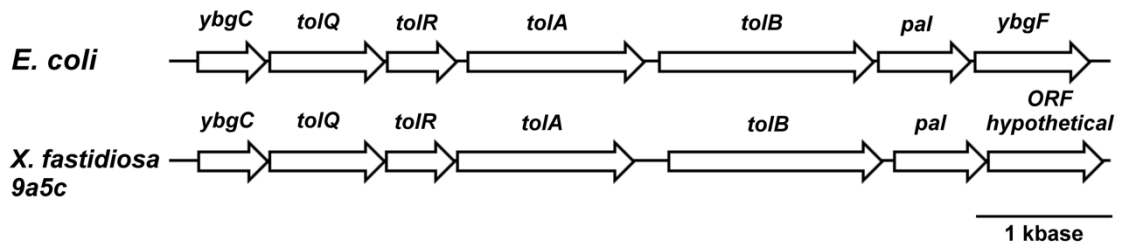
Supplemental Figure S1. Comparison of the organization of the *tol-pal* gene cluster in the *X. fastidiosa* 9a5c genome compared with the same region in the *E. coli* genome. Both operons exhibit the same gene structure and comprise a region of approximately 6 kb. The amino acids identity between the proteins of *X. fastidiosa* and *E. coli*, YbgC, TolQ, TolR, TolA, TolB and Pal are 42%, 49%, 31%, 15%, 42% and 48%, respectively. Additional data on the amino acids identity of YbgF see Fig. S2.

```
Xforf_hyp     -MRFWGSTFCVVAMALGTVAP---------SSAQMSSLADRVMALEQR-ASDPQVNIDLI 49
EcYbgF        MSSNFRHQLLSLSLLVGIAAPWAAFAQAPISSVGSGSVEDRVTQLERISNAHSQLLTQLQ 60
                 :    :   ::: :* .**           **.  .*: *** **:   :..*:  :*

Xforf_hyp     NQINDLRSQIRQMQGSIEEMQHGYEQLKQQSKDQYLDLDSRLKPIESGSVKEPSRVLANP 109
EcYbgF        QQLSDNQSDIDSLRGQIQENQYQLNQVVERQKQILLQIDS----LSSGGAAAQS----TS 112
              :*:.* :*:* .::*.*:* *:  :*: ::.*:  *::**     :.**..    *    ..

Xforf_hyp     ISQVSPSHFNQPIAMSEQSPNIHGDASALTISNEERIAYNVAFDALKN-SKYADAAELFL 168
EcYbgF        VDQSGAAASTTPTADAG-----TANAGAPVKSGDANTDYNAAIALVQDKSRQDDAMVAFQ 167
              :.*  ..:  . * * :       .:*.* . *.: .  **.*:  ::: *: ** *

Xforf_hyp     SFLQLYPNGVYTPNALYWLGESYYAMHDFVSAEAQFRSLLSRYPTHDKASGSLLKEALCQ 228
EcYbgF        NFIKNYPDSTYLPNANYWLGQLNYNKGKKDDAAYYFASVVKNYPKSPKAADAMFKVGVIM 227
              .*:: **:..* *** ****:  *    .  .*   * *:::..**.  **:.:::* .:

Xforf_hyp     ANQGKNDDAQHSLEQVLSQYPGTDAARLAQERLQSIKLSQAMR 271
EcYbgF        QDKGDTAKAKAVYQQVISKYPGTDGAKQAQKRLNAM------- 263
               ::*..  .*:    :**:*:*****.*: **:**:::
```

Supplemental Figure S2. Alignment of the amino acid sequence of the conserved hypothetical protein of *X. fastidiosa* 9a5c (Xforf_hyp; NCBI reference sequence: WP_010894361.1) and the YbgF protein of *E. coli* (EcYbgF; NCBI reference sequence: WP_021550465.1). Xforf_hyp and EcYbgF exhibit approximately 30% identity. The characters below the amino acid residues in the alignment indicate (*) identical amino acid residues, (:) residues with strongly similar properties, and (.) weakly similar properties. The sequence alignment was obtained using the CLUSTALW2 server (http://www.ebi.ac.uk/Tools/msa/clustalw2).
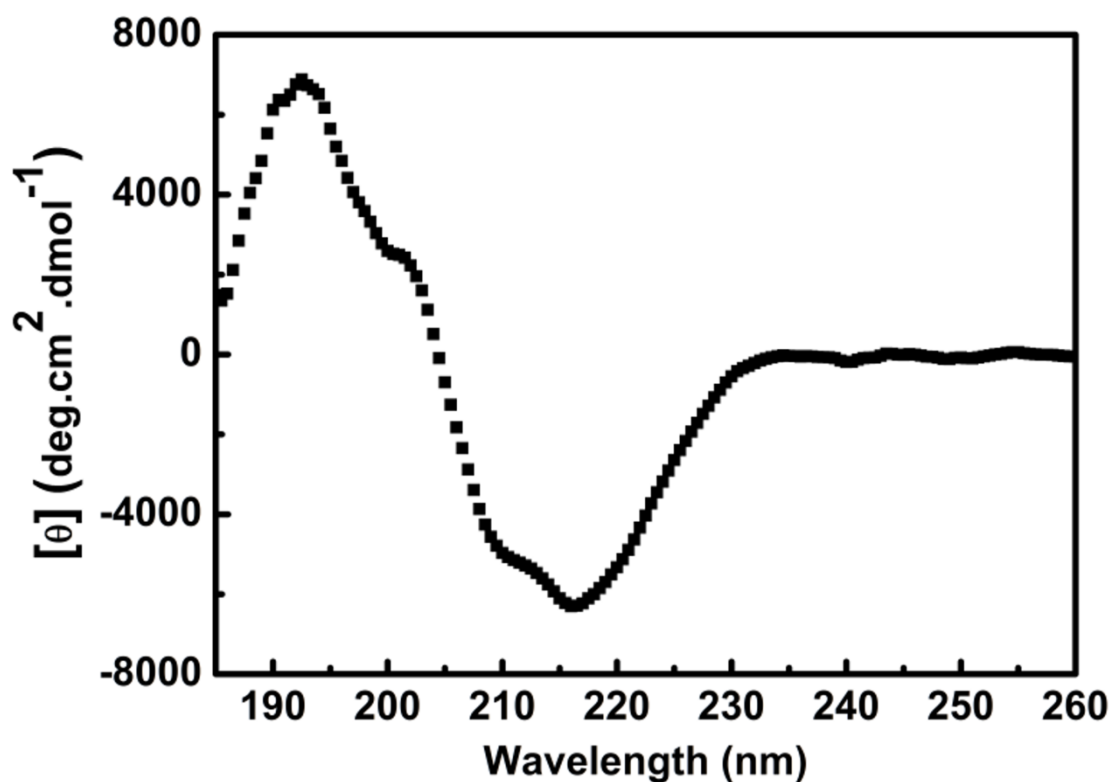
Supplemental Figure S3. Secondary structure content of the recombinant purified XfTolB as assessed by circular dichroism (CD). The CD measurements were performed using a JASCO J-810 spectropolarimeter (Tokyo, Japan) using quartz cuvettes with a pathlength of 0.1 mm. The CD measurements were performed at 24°C using samples of 4 µM protein in 10 mM sodium phosphate buffer, pH 8.0. The analysis and statistical deconvolution of the CD spectrum were performed using the DICRHOWEB server (http://dichroweb.cryst.bbk.ac.uk/).